Available online at www.sciencedirect.com
SCIENCE DIRECT®
ELSEVIER
Nuclear Instruments and Methods in Physics Research A 552 (2005) 513–521
NUCLEAR INSTRUMENTS & METHODS IN PHYSICS RESEARCH Section A
www.elsevier.com/locate/nima

The simulation of ultracold neutron experiments using GEANT4

F. Atchison[a], T. Bryś[a,d], M. Daum[a], P. Fierlinger[a,*], A. Fomin[b], R. Henneck[a], K. Kirch[a], M. Kuźniak[a,c], A. Pichlmaier[a]

[a]*Paul Scherrer Institut, Villigen, Switzerland*
[b]*Petersburg Nuclear Physics Institute, Gatchina, Russia*
[c]*Jagellonian University, Cracow, Poland*
[d]*ETH Zürich, Switzerland*

Received 28 September 2004; received in revised form 15 March 2005; accepted 24 June 2005
Available online 20 July 2005

Abstract

The GEANT4 code has been adapted to include the influence of gravity and inhomogeneous, slowly time-varying magnetic fields on neutrons. Ultracold neutrons (UCN) are introduced as a new class of particles. All relevant processes for the interactions at material boundaries and inside materials are implemented. The GEANT4 environment allows for an effective handling of complicated geometries.

PACS: 07.05.T; 28.20.C

Keywords: Ultracold neutrons; MC-simulation; GEANT4

1. Introduction

Neutrons with kinetic energies less than about 300 neV can be stored in material bottles and are referred to as ultracold neutrons (UCN). Their storage allows for studying fundamental problems of particle physics, concerning, e.g. the free neutron decay or the electric dipole moment of the neutron (for reviews, see Refs. [1,2]). Modeling of such experiments is indispensable if one wants to link an experimental observable, e.g. the storage time of an UCN trap to a material parameter like the loss probability per wall collision μ. The link is provided by the wall collision frequency and has to be calculated. UCN are strongly affected by gravitation and the codes have to take this into account. It is mainly for this reason that early efforts using kinetic gas theory or diffusion-type models have been abandoned and replaced by

*Corresponding author.
E-mail address: peter.fierlinger@psi.ch (P. Fierlinger).

0168-9002/$ - see front matter © 2005 Elsevier B.V. All rights reserved.
doi:10.1016/j.nima.2005.06.065

Monte Carlo (MC) calculations, which explicitly track single UCN trajectories and derive the quantity of interest from a high-statistics sample (see, Refs. [1, p. 99], [2, p. 95]). It is clear that the procedure can become extremely involved and time consuming when complex geometries and scattering conditions are to be handled. The requirement for the ballistic, analytical calculation of the trajectory from one wall collision to the next makes the introduction of realistic geometrical boundaries practically unmanageable. To our knowledge, existing simulations for UCN applications (e.g. see, Refs. [1, p. 99], [2, p. 95], [3,4]) are usually tailored and limited to simple and symmetric situations in order to give answers to specific questions. These codes are referred to as 'conventional' codes in the following.

We have chosen a different approach with the goal to implement UCN in an universal tracking code. GEANT4 [5] is a versatile, widely used toolkit for the simulation of the passage of particles through matter. Its application areas include high-energy and nuclear physics experiments, medical, accelerator and space physics studies. As such, it can handle many physically possible processes, including decay and particle production. The latter property is particularly interesting since it allows to combine the trajectory tracking of both, the 'parent' UCN as well as the 'daughter' decay products, e.g. in neutron decay experiments. It therefore appeared very tempting to exploit the GEANT4 advantages—versatility, completeness, easy geometry implementation and professional maintenance—and extend it to the case of UCN. The modified code will be referred to as GEANT4-UCN in the course of the paper and can be downloaded from the corresponding author on request via email.

In this paper the modifications of the code, its performance and an example application are given.

2. GEANT4 modifications

The additions to the code concern mainly the following areas: Section 2.1, new forces (gravity and time-varying, inhomogeneous magnetic fields), Section 2.2, new processes (UCN-specific reflection and scattering) and Section 2.3, new geometries.

2.1. Forces

Forces can be included easily, since GEANT4 makes provision for new forces through the specification of potentials. Although neutrons are of course treated in the standard GEANT4 package we have nevertheless introduced UCN as a new type of particle, being affected by gravity and magnetic fields. Gravity is implemented analogous to a constant homogeneous electric field for charged particles and is normalized such that the gravitational energy is $E_g = mgh = 102\,(\mathrm{neV/m})\,h$. The magnetic interaction is mediated by the magnetic moment of the neutron, $E_m = -\mu\mathbf{B} = \pm 60\,(\mathrm{neV/T})B$, where the sign is determined by the relative direction of the magnetic moment and the field. Thus, the force acting on the neutron can be written as $\mathbf{F} = \pm\mu\nabla|\mathbf{B}(\mathbf{r})|$ [6].

Arbitrary fields can be user defined and entered using functions for the calculation of the field strength in space and time. This allows field gradients to change arbitrarily and can cause inaccuracies if the field changes strongly within one step. If one uses field coordinates as an input, the interpolation between the field points is done linearly in space and time. An application for such fields is a magnetic shutter, as discussed in the example application given in Section 4, where the inhomogeneous field is switched from a value close to 0–1.5 T within several seconds as defined by the user.

2.2. Processes

UCN have long wavelengths with $\lambda \gtrsim 50\,\mathrm{nm}$. For material interactions it is therefore necessary to average over a large number of scattering centers. Coherent and incoherent scattering effects can be observed. The main implemented processes can in principle be separated into material boundary processes (reflection) and bulk material processes (scattering and absorption).

We first discuss reflection. Whether a UCN is reflected from the material depends on the neutron

energy E, its angle of incidence θ and the Fermi potential V. The Fermi potential is a material property depending on its density and the averaged bound coherent scattering length [1, p. 19], which is either calculated from the chemical composition of the material or implemented as a parameter. From this the critical velocity v_c of the material is calculated (corresponding to the maximum velocity for total reflection at normal incidence) and compared to the normal velocity component v_n. If $v_n < v_c$, the neutron will be reflected and different reflection models can be applied. We have implemented specular and diffuse reflection and the user can specify the probability for either process to happen (it should be noted that this is a simple practical approach, other models describing the influence of surface roughness are discussed, e.g., in [1, p. 31], [2, p. 100 and 184], which can be implemented by the user). For diffuse reflection we employ the usual cosine distribution for the reflected intensity, e.g. [1, p. 101]. The fact that even for total reflection there is a tiny probability for the neutron to get 'lost' is implemented via the material-dependent loss factor η. The latter is connected to the loss probability per wall collision μ which is a function of E, θ and V and is here written in terms of the normal component of the velocity on the surface v_n:

$$\mu(v_n) = 2\eta\left(\frac{v_n/v_c}{\sqrt{1-(v_n/v_c)^2}}\right) \quad (1)$$

(see, e.g. Ref. [1, p. 25]). Also other parameters useful for the simulation of storage experiments like e.g. the probability for 'spin-flip per wall reflection' β (independent of E, θ and V) have been implemented. Of course, β could also be made energy and angle dependent. The loss and spin-flip probability parameters are material properties and have to be implemented explicitly since theoretical approaches for the description of these phenomena could not be verified experimentally so far.

If the normal velocity component is larger than v_c, the particle can be reflected or it enters the material and can be elastically scattered, absorbed or up-scattered, i.e. inelastically scattered to energies above the UCN regime. Over barrier reflection is treated following Ref. [1, p. 21], with the amplitude of the reflected wave

$$R = \frac{\sqrt{E_\perp} - \sqrt{E_\perp - V}}{\sqrt{E_\perp} + \sqrt{E_\perp - V}} \quad (2)$$

with $E_\perp = mv_n^2/2$ and the probability for reflection $|R|^2$. The absorption is calculated in the usual way via an exponential attenuation law with the absorption cross-sections proportional to $1/v'$. Here v' is the velocity inside a material, where the normal component of the velocity vector is changed due to the index of refraction. Forces acting on a particle inside a material change its velocity and direction, which affects e.g. the mean free path inside the material. Thermal up-scattering is neglected here (but easily implemented), since for storage in material bottles the observed losses are not consistent with theoretical predictions [1], nevertheless user-defined scattering laws can be implemented. Elastic scattering is treated by calculating a mean-free path for the particle using user-defined scattering cross-sections. The index of refraction in the material is calculated by changing the component of the velocity normal to the surface using energy conservation (see, Ref. [1, p. 24]).

2.3. Geometries

The new implemented features are geometries that have time varying properties. An example is the definition of shutters, which are volumes that can change their material composition, as specified in a macro file. For instance, an arbitrary volume made of massive beryllium can change its properties to 'vacuum' and in this way simulate a mechanical UCN valve, a shutter or a chopper.

3. Code tests

3.1. Comparison with analytical trajectory calculations

A stringent test for the accuracy of the trajectory calculation is the comparison with analytical calculations. Within GEANT4, a particle is

propagated inside a field by integrating the equation of motion using a stepping algorithm. The advantage of such a method is that many problems that are difficult to integrate analytically can be solved much easier and it is therefore much more versatile. Examples are the propagation of a particle in a complex geometry, in a complicated field, or the proper behavior inside a material when forces are taken into account. The cost for the versatility is a longer calculation time compared to fully analytical trajectory calculation. Of the various algorithms provided in GEANT4, Runge–Kutta 4 turned out to be reasonably fast and stable. In order to optimize the tracking accuracy inside complicated geometries we use the 'miss-distance' parameter, Δ_{miss}, which is one of the standard accuracy parameters in the GEANT4 package. The trajectory of the particle is broken up into short linear segments with the length of the segments constrained by Δ_{miss}, which is the maximum allowed deviation of the linear track segment from the 'real' trajectory. The 'real' trajectory is estimated using the convergence of the stepping algorithm. For a given Δ_{miss} the linear path segment becomes shorter if the curvature of the trajectory is strong. A smaller Δ_{miss} increases the accuracy, but leads to longer calculation times.

We discuss three test-cases concerning the accuracy of the trajectory calculation: (a) in the gravity-only case a UCN with kinetic energy $E_{\mathrm{kin}} = 60\,\mathrm{neV}$ bounces on a horizontal mirror; (b) in the 'gravity with magnetic field' case a UCN experiences in addition to gravity an inhomogeneous magnetic field with a constant gradient of 15 T/m acting against gravity (see, Fig. 1, upper panel); (c) the neutron periodically enters and leaves the magnetic field, still in the presence of gravity (lower panel of Fig. 1). It should be noted that case (c) is a very stringent test which is almost impossible to prepare in reality since at the field boundary the gradient changes abruptly from 0 to 15 T/m. As mentioned above, the field boundary is not at a volume boundary and therefore the gradient change can occur within one step causing an additional position deviation.

Fig. 2 shows the accumulated position deviation in millimeter per meter flight-path as a function of the miss-distance parameter Δ_{miss}. The position

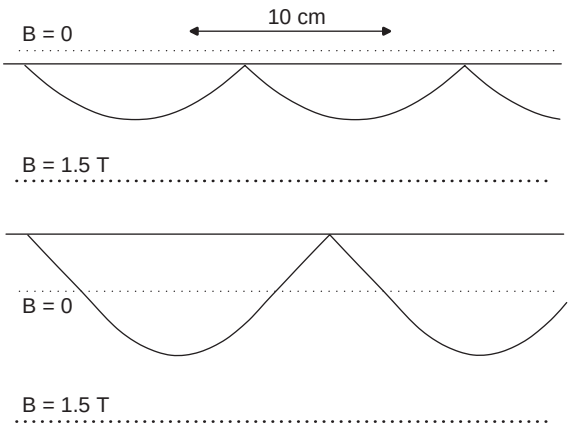

Fig. 1. UCN reflected by horizontal surfaces. The upper trajectory shows a neutron subject to gravity and to an inhomogeneous magnetic field (15 T/m) and being reflected from a horizontal surface above (case (b) in the text). The particle is started with a kinetic energy of 60 neV at a 45° angle in downward direction. Since both forces are independent of the vertical position the combined effect causes parabolic trajectories. For case (c) (lower trajectory) the reflecting surface is outside the magnetic field region and therefore the neutron sees two different force fields: one is due to gravity and the other due to the superposition of gravity and an anti-parallel magnetic field. Along the line $B = 0$ (thin dotted line) the field gradient changes abruptly from 0 to 15 T/m.

deviation is defined as the absolute value of the difference between the positions calculated by GEANT4 and analytically (for cases (b) and (c) the 'analytic' calculation was replaced by a GEANT4 calculation, where Δ_{miss} was set to 10^{-20} mm). To be useful for practical applications, the position deviation was determined from trajectory simulations with flight-times typically encountered in storage experiments, i.e. about 100 s, corresponding to about 1500 bounces for the case shown in Fig. 1. For a flight time of 5 s the position deviation is about five times smaller. This is because the position deviation caused by the curvature also leads to an angle deviation which accumulates over the periodic mirror reflections and produces a non-linear behavior with flight-time, depending on the gradient of the field. The position deviation is larger for case (c), where the UCN periodically enters/leaves the magnetic field region with a corresponding additional position deviation due to the finite segment length at the

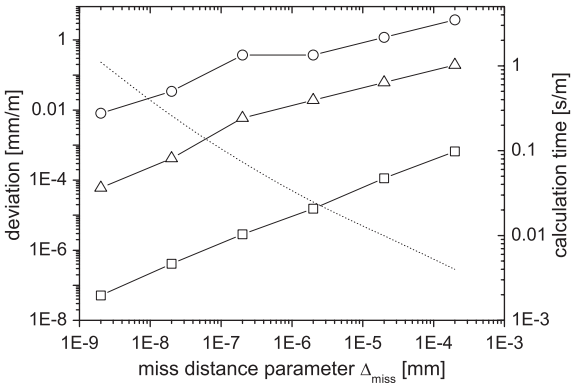

Fig. 2. Position deviation (left scale) and calculation time (right scale) per meter flight path as a function of the miss-distance parameter Δ_{miss}. The position deviation in millimeter per meter flight path is given for the cases discussed in the text: 'gravity-only', case a (squares), 'magnetic field with gravity', case (b) (triangles) and 'periodic magnetic field with gravity', case (c) (circles). The calculated data points are connected by solid lines to guide the eye. The calculation time (in seconds per meter flight path for—in this case—60 neV neutrons) also depends on the miss-distance and is given by the dotted curve without symbols and the right-hand scale.

field boundary. The calculation times given by the right ordinate are typical for a single CPU PC with 2.4 GHz. For comparison: tracking 10^4 particles in the standard GEANT4 example N02 took 50 s using minimum screen output. In order to achieve sufficient accuracy for extensive calculations with complicated magnetic field distributions the computing time may become a problem. To some extent the problem can be alleviated by approximating a measured field map by an analytical model with continuous functions.

It should be noted that tests a and b represent 'average' cases. Since the accuracy depends on the trajectory curvature and on the field inhomogeneity one would expect better accuracy for less-curved trajectories and less accuracy for highly curved trajectories. In that sense the position deviation estimates based on incidence angles of 45° are considered applicable to typical UCN storage and transport experiments.

As a final remark concerning accuracy, one should bear in mind that UCN experiments in general deal with statistical processes and only time-averaged or probabilistic quantities like storage time, wall collision frequency, spin-flip probability per wall collision, etc. are determined. As long as one does not deal with UCN 'range' spectrometers or UCN microscopy, inaccuracies for individual particle trajectories on the millimeter level are in most cases irrelevant. What counts is the statistical behavior of an ensemble of UCN streaming along a guide or moving at random in a storage vessel. It has to be surmised that the deviations mentioned are easily offset by inaccuracies introduced by the limited knowledge of the real reflecting surface morphology (see, also Ref. [1]) or of the geometry on a microscopic level.

3.2. Tests against conventional MC codes

Here, we discuss the comparison with conventional MC codes. Since there is no widely used standard conventional code we compare with the code of one member of our collaboration (A. Fomin) which has been used in many applications. This code starts from an initial distribution of neutrons and calculates the track of each particle analytically until it reaches a material boundary. At each wall collision the loss and reflection probability is calculated, resulting in a new direction to calculate the trajectory until the next boundary is reached. The surfaces are limited to flat, cylindrical and ellipsoidal. The neutron decays with a lifetime of 888 s. For the tests we used the same initial distributions, diffusion- and loss parameters. In the first test case we compare the velocity spectrum transformation through a simple guide system with $140 \times 140\,mm^2$ cross-section. It consists of a 2 m straight, horizontal section, followed by a 90° bend (1 m radius) and a 2 m straight, vertical section. The relevant parameters are: $v_c = 7.8\,m/s$ with no loss for $v_n \leqslant v_c$ and total loss for $v_n > v_c$, 0.7% diffuse reflection probability, incident velocity components v_{axial} are distributed with a linearly increasing probability from 0 to 15 m/s and v_{radial} has a constant probability between 0 and 7.8 m/s normal to the guide wall at the entrance. The results are shown in Fig. 3. The velocity spectrum transformation was defined as the number of UCN in a given total velocity bin (e.g. at 5 m/s) after transmission through the system divided by the number of UCN in the

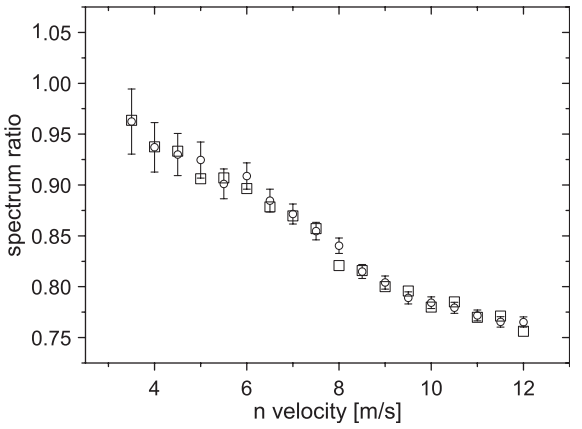

Fig. 3. Comparison of two guide 'transmission' calculations. The total velocity spectrum transformation through the guide is described in the text, calculated by GEANT4-UCN (open circles) and by the code of A. Fomin (squares).

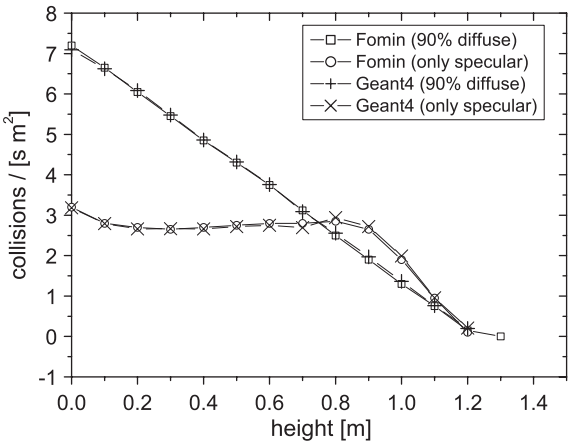

Fig. 4. Wall collision frequency as a function of height, calculated with GEANT4 and with the code of A. Fomin. Two different reflection conditions were considered: specular reflections only (open circles and x-crosses) and 90% diffuse and 10% specular (open squares and +). For further detail see text.

same total velocity bin (i.e. again at 5 m/s) at start. Please note that this is not a transmission vs. velocity curve in the usual sense. Within statistics the agreement between both predictions is good.

In a second example, UCN are stored inside a cylindrical beryllium bottle of radius 250 mm and height 2700 mm ($v_c = 6.8$ m/s). The neutrons are produced uniformly at the bottom within a circular area with 200 mm radius around the center. The UCN are mono-energetic (131 neV, corresponding to $v = 5$ m/s or a height of 1.29 m) and are started with a certain angular distribution. We consider two cases with the wall reflections either being completely specular or 90% diffuse and 10% specular. In Fig. 4, the distribution of wall collisions along the vertical direction is plotted for the two cases. Each curve involves the tracking of 10^5 neutrons. The agreement between both calculations is perfect. Physically, the two curves represent two extreme cases: with 90% diffuse reflection probability the directions of the neutrons get immediately randomized. Under these conditions the neutrons can be adequately described by kinetic gas theory with inclusion of gravity and the wall collision frequency is linearly decreasing with height [1]. With purely specular reflection on the other hand, the UCN 'memorize' the initial angular distribution to some extent and the wall collision frequency depends on the details of the geometry and of the initial angular distribution.

As a third example, we test the tracking of the polarization vector in a magnetic field. In a process that can be chosen by the user on demand, the position of the polarization vector in a field is calculated at the end of each geometrical step. This is done in a similar way as it is described in Ref. [7]: it is based on a Runge–Kutta 4 algorithm with angular coordinates used for tracking and an adaptive step size algorithm for the accuracy of tracking. In our implementation, the adaptive step size divides the geometrical step into smaller segments, where the number of segments arises from the chosen accuracy parameter. In the testcase, we consider a 1×10^{-4} T homogeneous magnetic field along the y-axis, which rotates around the z-axis with a frequency ω by $\pi/2$ to the x-axis. The ratio of the Larmor-frequency $\omega_L = 2\mu|\mathbf{B}|/\hbar \sim 3$ kHz and the precession frequency ω of the field is here called the adiabaticity coefficient [7]. In Fig. 5, a comparison of results from the analytical solution given by Ref. [7] and the simulation using GEANT4 is shown. The initial orientation of the polarization vector is parallel to the magnetic field vector $(x = 0, y = 1, z = 0)$. After a rotation of the field vector by $\pi/2$ around

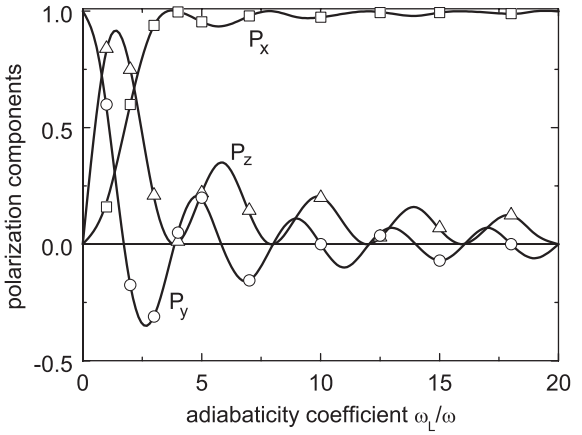

Fig. 5. Components of the polarization vector after a rotation by $\pi/2$ of a 1×10^{-4} T magnetic field. On the abscissa, the ratio of the Larmor-precession and the rotation frequency of the field is shown. The squares, triangles and circles correspond to the components of the polarization vector P_x, P_y and P_z from the GEANT4 simulation, while the fully drawn curves are the results from the analytical calculation taken from Ref. [7].

the z-axis the orientation of the vector becomes $(x = 1, y = 0, z = 0)$ in the adiabatic limit $(\omega_L \gg \omega)$, again parallel to the magnetic field.

4. A magnetic shutter as an example application

This example combines storage in a vessel with the influence of a slowly time-dependent magnetic field. The practical application is a magnetic shutter. With respect to simulation this represents a considerable challenge, since—in addition to tracking UCN with gravity—it also requires to handle inhomogeneous time varying magnetic fields. A holding field along the tube (~5 mT), which does not influence the tracking, assures that the adiabatic condition is fulfilled over the whole volume and no spin-flips occur. The simulated setup is shown in Fig. 6. The storage tube is 1 m high, has a diameter of 70 mm and is assumed to be made of Be, i.e. $v_c = 6.8$ m/s and a low wall loss probability. The plane of the maximum magnetic field strength is located at $z = 0$. The magnetic field can be turned on and off with a ramp of 3 s, it is switched off for filling and switched on for storage. Filling is simulated by creating UCN

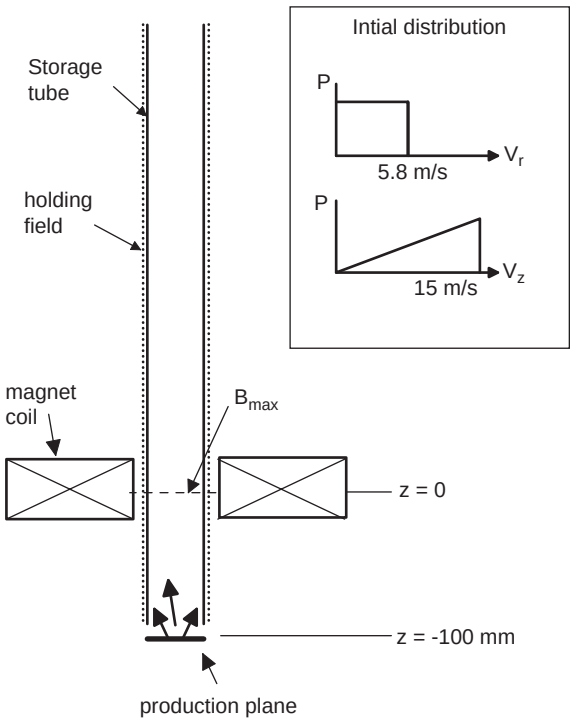

Fig. 6. Scheme of the magnetic storage example. The inset box shows the probability distribution of the velocity components of the produced neutrons. v_r denotes the radial component, v_z the vertical component, the probability for higher velocities in z is rising linearly.

homogeneously over a production plane at $z = -100$ mm with the momentum distributions shown in Fig. 6. Neutrons can freely enter and leave the storage volume which extends from the plane of the maximum magnetic field to the open top end of the sample tube. The filling time depends on the balance between incident flux and losses. As can be seen from Fig. 7 the neutron density inside the storage volume reaches equilibrium after about 2 s. The figure also demonstrates the delicate influence of mechanical slits in the guide system on the obtainable density inside the sample. At $t = 3$ s filling is stopped and the UCN drop out of the tube with a time constant similar to that for filling.

The ramping of the magnetic field was simulated using a linear function of the amplitude from the value of the holding field to $B_{max} = 1.5$ T (corresponding to a maximum storable energy of 90 neV) at $z = 0$ mm over a period of 3 s. The gradient of

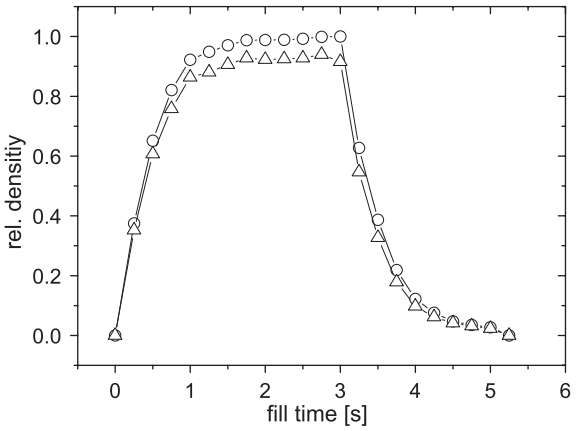

Fig. 7. The relative density of neutrons inside the storage tube after starting the filling at $t = 0$. After about 2 s an equilibrium state is reached, the achievable density depending on the incident neutron flux and the losses. The density reduction caused by the consideration of an annular slit with 2 mm height around $z = -20$ mm and 100% absorption is demonstrated by the triangles.

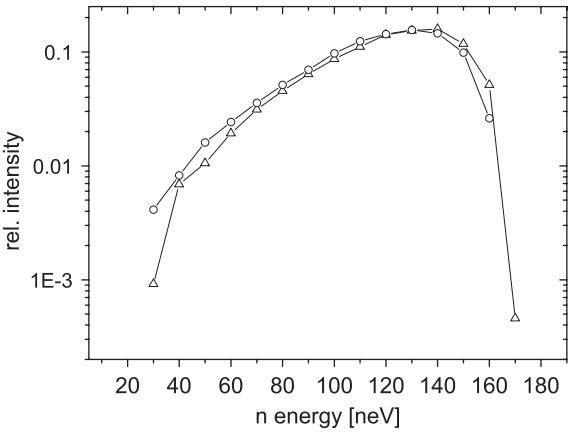

Fig. 8. The effect of the time-dependent field on the stored total energy spectrum (gravitational plus magnetic plus kinetic energy):initial spectrum (open circles), spectrum 5 s after switch-on (open triangles).

the inhomogeneous field is 15 T/m from $z = -100$ mm to $z = 0$ and -15 T/m from $z = 0$ to 100 mm. Only UCN with energies below 90 neV and a magnetic moment orientation anti-parallel to the magnetic field direction can be stored for longer times. In addition, the increase of the field strength with time causes an energy gain of the stored UCN according to the magnetic interaction. The energy gain depends mainly on the time the neutron spends in the region of increasing field and the time derivative of the field. Therefore, slower UCN which spend more time in the field gain more energy than faster ones (see Fig. 8). The mean energy gain for the full storable spectrum (i.e. below 90 neV) is about 4%, which leads to a systematic correction for the mean wall collision frequency by 2%. It turns out that the modification of the energy spectrum depends only weakly on the ramping time, at least for times between 2 and 5 s. An interesting quantity is the distribution of the wall collision frequency depending on the height inside the storage volume, shown in Fig. 9. Neutrons with higher energies reach deeper into the magnetic field and also reach higher positions inside the storage volume.

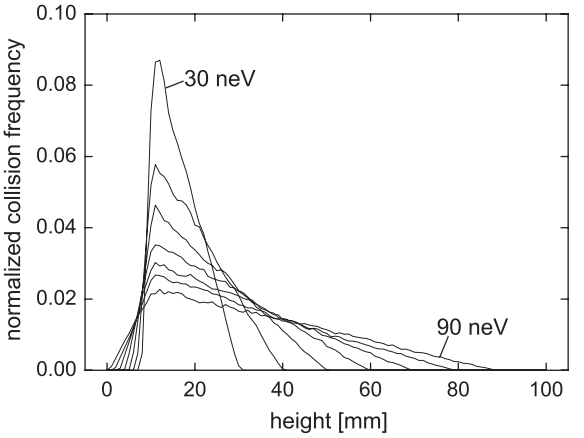

Fig. 9. Wall collision frequencies as a function of height in the bottle. The energies shown are from 30 to 90 neV. The different curves are normalized to the same area. The averaged wall collision frequencies for the different energies are (30 neV, 21.7 Hz), (40 neV, 26.4 Hz), (50 neV, 30.8 Hz), (60 neV, 34.3 Hz), (70 neV, 37.9 Hz), (80 neV, 40.7 Hz), (90 neV, 43.6 Hz).

The full simulation—of which only a few aspects have been discussed here—is used in an experiment for the determination of the loss- and depolarization probability per wall collision currently performed at the Institute Laue Langevin, Grenoble [8].

5. Conclusion

Additions to the GEANT4 code have been made to handle the influence of gravity, inhomogeneous and slowly time-dependent magnetic fields on the trajectories and UCN-specific processes with respect to surfaces and material interactions. In contrast to existing codes concerned with tracking UCN this code can handle almost any geometry. Its performance has been extensively tested and it is ready to simulate a wide variety of UCN experiments.

Acknowledgements

The work was performed at the Paul Scherrer Insititut, Villigen, Switzerland. We appreciate fruitful discussions with L. Desorgher concerning the GEANT4 code.

References

[1] R. Golub, D.J. Richardson, S.K. Lamoreaux, Ultra-cold Neutrons, Adam Hilger, Bristol, Philadelphia, New York, 1991.
[2] V.K. Ignatovich, The Physics of Ultracold Neutrons, in: Oxford Series on Neutron Scattering in Condensed Matter, Clarendon Press, Oxford, 1990.
[3] G.F. Gareeva, et al., Nucl. Instr. and Meth. A 369 (1996) 180.
[4] C. L. Morris, et al., Phys. Rev. Lett. (2002) 272501.
[5] S. Agostinelli, et al., Nucl. Instr. and Meth. A 506 (2003) 250.
[6] J.D. Jackson, Classical Electrodynamics, Wiley, New York, London, Sydney, 1962.
[7] P. Seeger, L.L. Daemen, Nucl. Instr. and Meth. A 457 (2001) 338.
[8] T. Brys, et al., Nucl. Instr. and Meth. A, 2005, in press.